Photothermal Methods for Single

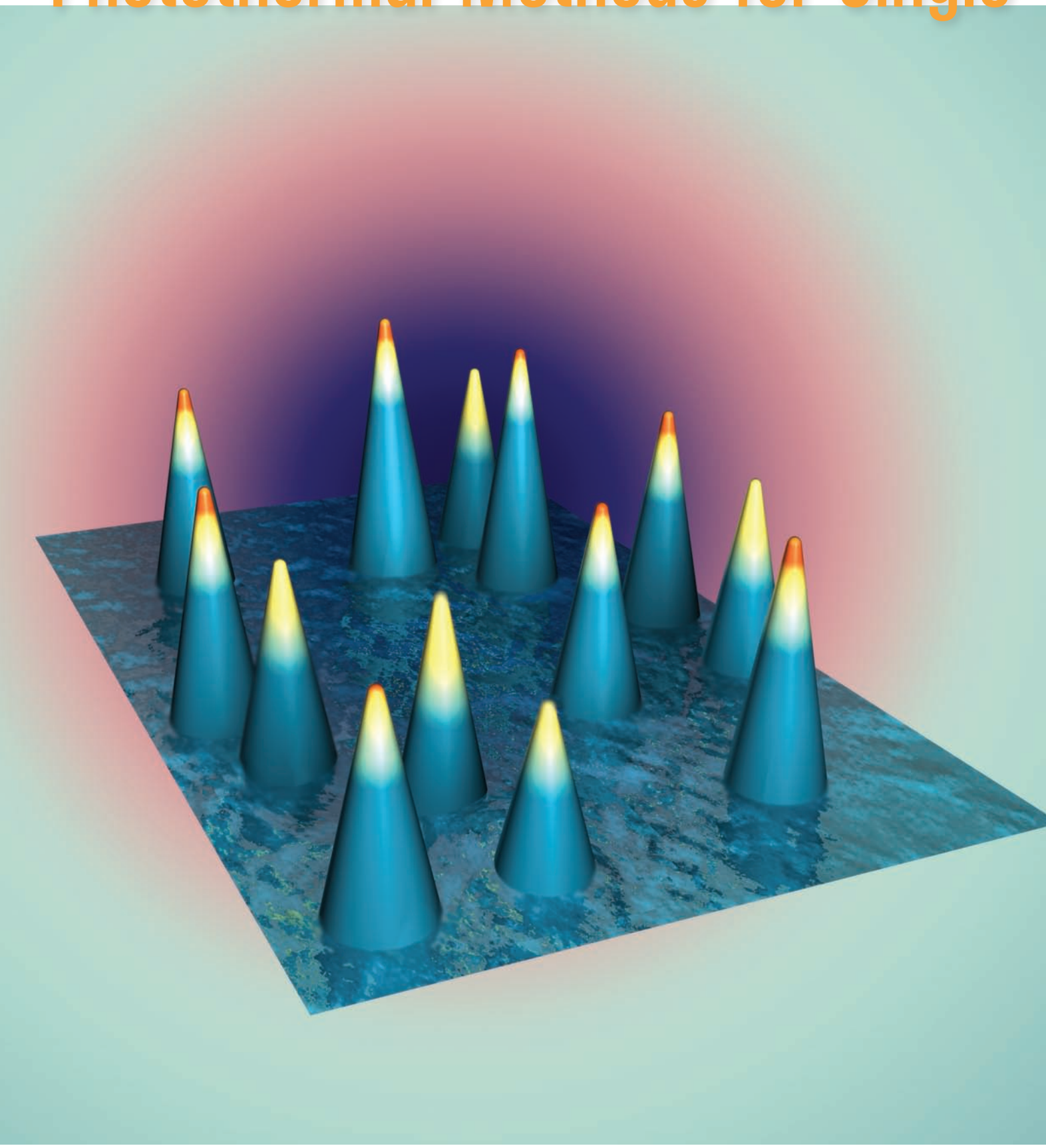

Nonluminescent Nano-Objects

Laurent Cognet
Stéphane Berciaud
David Lasne
Brahim Lounis
Université Bordeaux 1 and Centre National de la Recherche Scientifique (France)

New optical methods allow the detection of tiny individual nano-objects, opening a wide range of applications.

In the rapidly evolving field of nanoscience, where size is a crucial determinant of the properties of an object, simple and sensitive methods for the detection and characterization of single nano-objects are needed. Electron microscopy or near-field methods such as scanning tunneling microscopy and atomic force microscopy provide atomic resolution, but they require extensive sample preparation and are not ideal in a complex environment such as biological matter. Far-field optical methods have the advantages of requiring no contact and being minimally invasive.

The most commonly used optical techniques are based on luminescence. Currently, single fluorescent molecules are applied routinely to research domains ranging from quantum optics to life science. Yet, the intrinsically limited photostability of the objects restrains the applicability of fluorescence microscopy. Traditionally, optical studies of nonfluorescing nano-objects—for instance, metal nanoparticles (NPs)—are based on intensity scattering. However, such techniques are generally limited to detecting relatively large particles; this is because of background scatter and the sharp decrease in the scattered intensity as the objects get smaller. Consequently, new methodologies recently have been developed to allow the detection of very small nonluminescent nano-objects in complex environments.

Detection of nonfluorescing nano-objects

Several traditional approaches exist for the far-field optical detection of individual nonluminescent nano-objects. These methods are based on scattered intensity or on the particle generating new wavelengths, either in a linear photoluminescence process or in nonlinear processes (*1*–*4*). A general review of these methods applied to metallic NPs can be found (*5*). In this article, we first consider the case of gold NPs (AuNPs) of diameter D, which is much smaller than the wavelength of light λ, and then discuss other types of absorbing nano-objects.

In conventional scattering methods, the intensity of the field elastically scattered by a single NP is usually spatially separated from the exciting field by particular geometrical arrangements, as with dark-field or total internal reflection microscopy, and detected in the far-field region. However, because the polarizability of an NP is proportional to its volume, the intensity scattering cross section of the particle varies as D^6, whereas its absorption cross section varies as D^3 and dominates for small sizes. For example, for gold spheres in water probed by 532 nm laser light, absorption is more important than scattering for $D < 100$ nm.

To detect such small particles, one can measure the direct absorption or use the interference of the scattered field with a reference field to get a signal that, similar to absorption, varies with D^3. Because of the amplification by the reference wave, such interferometric techniques not only result in high sensitivity but also can provide the amplitude and the phase of the scattered wave. A review dedicated to these scattering- and absorption-based methods was published recently (*6*).

In the next sections, we present methods based

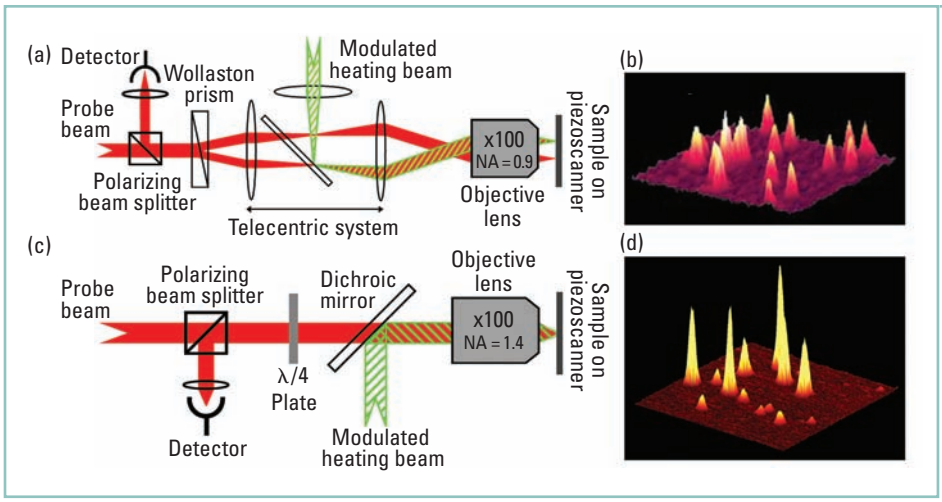

FIGURE 1. Experimental schemes for the detection of individual nano-objects.

(a) Instrumental setup for PIC. (b) PIC image of a 10 × 10 μm region of sample containing individual 5 nm AuNPs. (c) Instrumental setup for PHI. (d) PHI image of a 10 × 10 μm region of sample containing a mixture of individual 2 nm (short peaks) and 5 nm (tall peaks) AuNPs.

on the photothermal effect. These are the most sensitive ones to date and have the advantage of being useful in highly scattering environments, which makes them suitable for a broad range of applications.

Photothermal interference contrast method

When excited near their surface plasmon resonance (SPR), metal NPs have a large absorption cross section and exhibit a fast electron–phonon relaxation time in the picosecond range, which makes them very efficient light absorbers (*7*). Because the luminescence yield of these particles is extremely weak, almost all of the absorbed energy is converted into heat (*8*). The increase in temperature induced by this absorption gives rise to a local variation of the refractive index. This photothermal effect can be used to detect and study the NPs.

Photothermal detection was proposed by Tokeshi et al., who used a thermal lens effect to detect very low concentrations of absorbing molecules in liquid solutions (*9*). Boyer et al. designed a highly sensitive polarization interference method called photothermal interference contrast (PIC) for the detection of the small changes in the refractive index around an absorbing particle (*10*). The experiment was performed by using a combination of two lasers. The NPs were heated by the 514 nm line of an argon ion laser with its intensity modulated at high frequency. The horizontally polarized output of a HeNe laser (633 nm wavelength) was split by a Wollaston prism into two perpendicularly polarized beams, forming the two arms of the interferometer (probe and reference). The probe beam (HeNe laser) was overlaid with the heating beam (argon laser), and the two arms of the interferometer were sent to a microscope objective via a telecentric lens system.

The probe and reference beams that were back-reflected by the sample recombined in the Wollaston prism and were then reflected by a polarizing beam-splitter cube onto a fast photodiode (Figure 1a). A lock-in amplifier detected the variations of the red intensity and thus determined the phase difference between the two red beams at the modulation frequency of the green beam. Microscopic images were obtained by scanning the sample with respect to the three spots. With PIC, images of AuNPs as small as 5 nm in diameter embedded in thin polymer films were recorded with S/N > 10 (Figure 1b). The inventors also showed that, in addition to its intrinsic sensitivity, the PIC method is remarkably insensitive to the scattering background, even that which arises from strong scatterers such as 300 nm latex beads. Using a modified PIC setup to image NPs in thick samples, Cognet et al. detected single proteins labeled with individual 10 nm AuNPs on the surfaces of fixed cells (*11*).

Although the sensitivity of the PIC method is high, it could not reach the shot-noise limit. Indeed, the use of high-numerical-aperture objectives induced depolarization effects that degraded the quality of the overlap between the two arms of the interferometer. As a consequence, the detection of NPs with PIC required relatively high laser intensities (~10 MW/cm^2), which can be a serious limitation for many applications, such as in biology.

Photothermal heterodyne imaging

Berciaud et al. then developed a more sensitive method called photothermal heterodyne imaging (PHI), also called laser-induced scattering around a nanoabsorber (LISNA) for biological applications (*12–15*). It combines a time-modulated heating beam and a nonresonant probe beam that overlap on the sample. The probe beam produces a frequency-shifted scattered field as it interacts with the time-modulated variations of the refractive index around the absorbing NP. The scattered field is then detected by a photodiode through its interference with the probe field, which acts like a local oscillator as in any heterodyne technique (Figure 1c). This signal is extracted from the beat note at the modulation frequency by lock-in detection.

In practice, PHI can be shot-noise-limited because it does not suffer from the limitations inherent to PIC. Its sensitivity is more than 1 order of magnitude higher than that of any other method (Figure 1d). This sensitivity enabled the unprecedented detection of individual gold clusters as small as 1.4 nm in diameter, which contain <100 atoms.

Single-metal NP absorption spectroscopy

Noble metal NPs are strong absorbers and scatterers of visible light because of SPR. The corresponding resonant peak energies and line widths are sensitive to the NPs' size, shape, and nanoenvironment. For rather large metal NPs ($D \geq 20$ nm), the resonant peak energy of the SPR experiences a redshift as size increases, which is caused by retardation effects and increasing contributions from multipolar terms. In addition, for NPs with $D > 50$ nm, radiative damping of the collective electronic excitation strongly broadens the line width of the SPR.

However, for NPs significantly smaller than the electron mean free path (D < 20 nm), these extrinsic size effects become negligible and intrinsic size effects prevail (*16*, *17*). In a classical interpretation, the resulting limitation of the electron mean free path and interactions with the surrounding matrix are responsible for additional damping at the NPs' surface (*16*, *18*). In the time domain, this translates into a large reduction of the surface plasmon dephasing time to a few femtoseconds. As a consequence, because of these additional size-dependent damping processes, the dielectric constant of small NPs can no longer be described by the bulk metal values.

Experimental studies on ensembles of metallic NPs revealed the existence of such effects (*16*, *19*). However, comparisons between theory and ensemble measurements are still a matter of debate, because the inhomogeneities in NP size, shape, and local environment experimentally blur the homogeneous width of the SPR.

To circumvent this shortcoming, PHI was used to record absorption spectra of individual AuNPs with D as small as 5 nm with excellent S/N (*20*). Figure 2a shows the absorption spectra of two individual AuNPs with D = 33 nm and 5 nm taken in the 515–580 nm range. The peak resonance energies are affected weakly by intrinsic size. In contrast, a significant increase in the width of the resonance clearly appears and cannot be explained by Mie's theory and the bulk values of the gold dielectric constant. Good agreement was found between the experimental widths and Mie simulations with size-dependent corrections (*20*; Figure 2b).

Although the existence of intrinsic size effects in the optical response of AuNPs was revealed unambiguously, some of the damping processes are caused by interband transitions. Consequently, the plasmon spectra of individual AuNPs are asymmetric, and it is a delicate process—if not impossible for very small particles—to define an fwhm of such an absorption spectrum. This makes it difficult to connect the widths of the plasmon resonances to the damping rate.

To avoid the contribution of interband transitions in the measured spectra, the plasmon resonance frequency could be redshifted by embedding gold nanospheres, gold nanorods, or core-shell NPs in a high-index matrix (*21*, *22*). Another possibility is silver nanospheres, because their resonant energies are well separated from interband transitions. A drawback of silver particles, however, is that they have weak photostability caused by photooxidation (*3*). Interestingly, the reactivity of silver particles can be reduced by encapsulation with polyethylene glycol (PEG) (*23*). Berciaud et al. detected individual PEG-coated silver NPs with an average D = 5.3 nm by PHI (*13*). The size distribution, however, was broad. For these experiments, a modulated diode laser emitting at 405 nm with an intensity of ~50 kW/cm^2 was used as a heating source. As expected, the signal was ~10× higher than that of AuNPs of the same size. When it becomes possible to synthesize silver NPs with a narrow size distribution, a quantitative study of the SPR of individual silver NPs with D < 5 nm should be feasible.

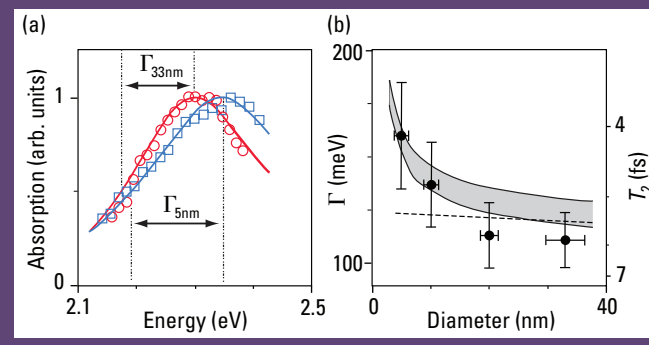

FIGURE 2. (a) Normalized absorption spectra of two single AuNPs of D = 33 nm (red) and 5 nm (blue). The extracted width at half-maximum is shown on both NP spectra. The experimental spectra are compared with simulations based on Mie theory (solid lines) with a size-dependent modification in the dielectric constant of gold. (b) Size dependence of the plasmon resonance width and the corresponding dephasing time. Experimental data (circles with SDs) are compared with Mie theory without (dotted line) and with (gray area) a size-dependent correction. The gray area accounts for the experimental uncertainties on the bulk dielectric function of gold.

Quantum dots

Interestingly, PHI can also be used to detect semiconductor nanocrystals made of CdSe–ZnS. These nano-objects have relatively high absorption cross sections (~10^{-15} cm^2), and when they are excited with sufficiently high intensities, excitons are created at average rates significantly higher than their radiative recombination rates (*24*–*26*). In this regime, efficient nonradiative Auger recombinations of the prepared multiexcitons occur (*27*). In CdSe–ZnS nanocrystals, these processes occur in picoseconds, as measured in ensemble time-resolved experiments (*28*). Thus, individual nanocrystals could be detected through their absorption by using PHI (*12*).

Contrary to luminescence, the photothermal signals do not show any blinking behavior. They remain stable over timescales longer than those necessary to record an absorption spectrum. Luminescence spectra were recorded in the monoexcitonic regime at low continuous-wave excitation intensities; photothermal absorption spectra were recorded in the high continuous-wave excitation regime, where excitons are created at average rates significantly higher than the radiative recombination rate of the band edge exciton. Luminescence from monoexcitonic recombination is very weak, and the prepared multiexcitons relax rapidly through efficient nonradiative Auger processes. The observed photothermal absorption bands were assigned to biexcitonic and charged excitonic (trionic) states. Complementary measurements of the photoluminescence spectra of the same nanocrystals led to the measurement of spectral Stokes shifts that were free from ensemble averaging and to an estimation of the biexciton and trion binding energies, which were in good agreement with previous experimental results (*29*).

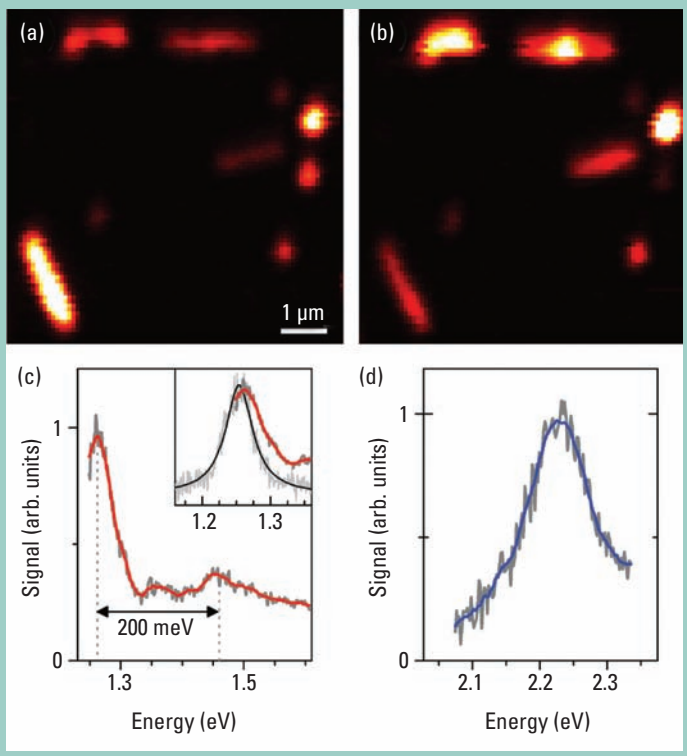

FIGURE 3. (a, b) PHI images of a region (8 × 8 μm) of a sample containing micrometer-sized nanotubes spin-coated on a glass slide. The orientation of the heating beam's polarization was vertical in (a) and horizontal in (b). The polarization-dependent absorption of SWNTs is evident, and the highest absorption is achieved when the SWNT longitudinal axis is parallel to the incident laser field. (c) Absorption (gray, raw data; red, smoothed data) and luminescence (black, Lorentzian fit) spectra of the first optical transition of an individual (6, 5) semiconducting SWNT. The large spectrum indicates the 200 meV sideband above the main absorption peak. The inset is the absorption spectrum around the main peak and the corresponding luminescence spectrum. (d) Absorption spectrum of an individual metallic nanotube (gray, raw data; blue, smoothed data).

Single-walled carbon nanotubes

All current methods for producing single-walled carbon nanotubes (SWNTs) lead to heterogeneous samples containing mixtures of metallic and semiconducting species with a variety of lengths and defects. This diversity of structures complicates precise spectroscopic characterization. Single-particle methods thus appear valuable for eliminating the heterogeneity present in bulk SWNT optical spectra. The optical properties of individual semiconducting SWNTs can be studied with their intrinsic NIR luminescence (*30*, *31*). Although sensitive, this approach is not universal, because only isolated semiconducting SWNTs exhibit such luminescence (*32*). Rayleigh scattering spectra from individual metallic and semiconducting SWNTs were obtained concurrently, but this technique has been applied only to long SWNTs with $D = 2$ nm individually suspended over open apertures (*33*).

PHI, however, can detect a priori semiconducting and metallic SWNTs in complex environments (*12*). More specifically, SWNTs have absorption cross sections of 10^{-18} cm^2/carbon atom and rapid inter- and intraband carrier relaxation dynamics (*34*, *35*). Metallic nanotubes have electron–electron and electron–phonon relaxation times in the subpicosecond range; semiconducting species have nonradiative decay times in the picosecond range, which are associated with weak ensemble luminescence quantum yields of ~0.01 (*32*, *35*, *36*). Figures 3a and 3b show high-S/N images of SWNTs obtained with PHI by using two perpendicularly polarized excitations. The structural identification of both semiconducting and metallic individual SWNTs was done from their absorption spectra at the first and second optical resonances. As expected for semiconducting nanotubes, exciton–phonon sidebands involving the Raman G band were observed at ~200 meV above the first optical resonance (Figure 3c). No such sidebands were detected at the lowest transition of metallic nanotubes (Figure 3d).

Biosciences

In a first demonstration, Blab et al. showed PHI's potential to provide a new readout strategy for DNA microarrays based on AuNPs (*14*). The determination and exact quantification of gene expression is becoming increasingly important in basic pharmaceutical and clinical research. Fluorescence-based DNA assays are most widely used but suffer from autofluorescence in some biological samples and substrates; this severely interferes with the detection of target molecules. DNA assays based on AuNP labels present a viable alternative. PHI commonly uses AuNPs >40 nm, which can be readily detected because of their strong light scattering at visible wavelengths (*1*, *2*).

To obtain increased specificity and reactivity, AuNPs with $D < 40$ nm are preferred. Indeed, small AuNPs functionalized with oligonucleotides exhibit a very sharp thermal denaturation profile, and the rate of reaction on a surface is much higher than that of large particles (*37*–*39*). Because small AuNPs ($D < 40$ nm) barely interact with light, their direct optical detection has been impossible without silver staining until recently (*37*, *39*). However, saturation at the amplification step limits the linear dynamic range because the typical size of the silver crystals is much larger than that of the AuNPs (*38*). Furthermore, spontaneous conversion of silver solution into metallic grains can occur, leading to nonspecific signals (*38*). Another alternative is the electrical detection of AuNPs after catalytic or enzymatic deposition of the silver (*40*, *41*). In this context, the possibility of detecting tiny AuNPs at the single-particle level holds great promise for new and more efficient optical readout schemes of DNA assays.

PHI was thus applied to standard, low-density, spotted DNA microarrays to avoid the use of silver enhancement techniques. These arrays are well suited for routine applications be-

cause they contain a limited number of genes (usually <1000), which enables good spotting quality and good reproducibility (*42*). PHI provides a reliable quantification of the amount of DNA hybridization in each spot of the microarrays (Figure 4). This determination is no longer limited by any constraints of the detection method. The only limitations are the degree of unspecific signals for low NP surface densities and the size of the AuNPs for high surface densities. Indeed, because all the AuNPs are detected (Figure 4b), the lower detection limit of DNA depends only on unspecific DNA hybridization events and on the quality of surface treatments. The upper detection limit is determined by the condition of weak plasmon coupling between particles. When the average distance between the small AuNPs is comparable to their size, the optical response of AuNPs is modified (*43*). Furthermore, the possibility of detecting much smaller AuNPs (D = 1.4 nm) should increase the dynamic range obtained with 20 nm AuNPs significantly (Figure 4c; *12*).

In addition to high sensitivity and dynamics, AuNP-based DNA arrays can be stored for long periods and remeasured several times. This approach thus combines the advantages of fluorescence measurements—small marker size and purely optical detection—with the high stability, specificity, and dynamic range afforded by AuNP labeling techniques and makes it promising for application in biochips.

Live-cell studies

The movements of molecules in the plasma membrane of living cells are characterized by their diversities, in both the temporal and spatial domains. Membranes exhibit a constitutive complexity, consisting of several different lipids and a great variety of proteins with highly dynamic and compartmentalized spatial distributions. These molecules explore the plasma membrane in various lateral diffusion modes and frequently interact with one another at specific locations to transmit information across the membrane, starting the cascades of specific signaling processes. Those molecular interactions are by nature heterogeneous, making ensemble observations of these phenomena rather challenging.

Single-molecule detection has allowed the elimination of the implicit averaging of conventional optical observations. Two main approaches have been used to track individual molecules in the plasma membrane of live cells, each with distinct advantages and limitations. Single-particle tracking (SPT) uses labels large enough (~40 nm AuNPs or even bigger latex beads) to enable the detection of Rayleigh intensity scattering by conventional microscopes (*44*). SPT permits researchers to follow the movement of individual molecules for a very long time and possibly at very fast imaging rates (*45*). SPT, for instance, revealed barriers set for diffusion by the cytoskeleton and the diversity of lateral diffusion modes of receptors for neurotransmitters in live neurons (*46*, *47*). However, the main drawback is the size of the beads, which might sterically hinder the interaction between the labeled molecules or alter their movements in confined environments, such as synaptic clefts or endocytotic vesicles.

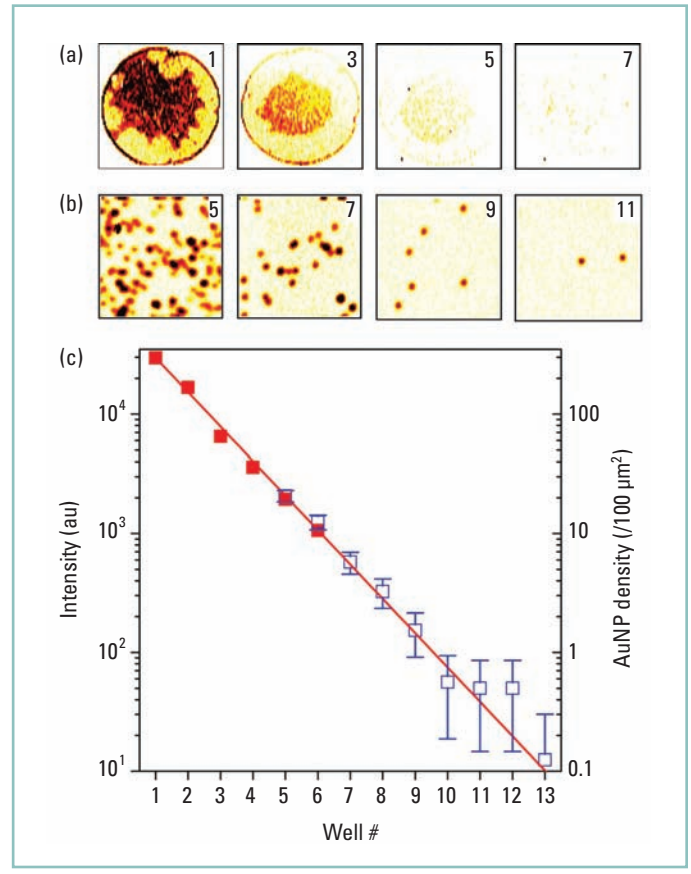

FIGURE 4. Imaging of DNA microarrays based on AuNPs.

Direct imaging (no silver enhancement) of four spots of a microarray by PHI at (a) low and (b) high resolutions. (c) Low (red) and high (blue) resolution; the corresponding AuNP densities in each spot are given on the right axis.

Single-molecule tracking (SMT) uses fluorescent organic dyes or autofluorescent proteins. Because these fluorophores are generally smaller than the target molecules, they do not have the drawback of SPT mentioned in the previous paragraph. In the neurosciences, SMT has revealed the lateral diffusion of glutamate receptors inside the synapses of live neurons (*48*). The main limitation encountered in SMT studies is photobleaching, which severely limits the observation time of a single fluorophore to typically <1 second in live cells.

An experimental technique that combines the advantages of SPT and SMT, namely long observation times and nanometer-sized labels, would thus have great potential. For biological questions, it would permit the recording of the full history of proteins in cells, including intermediate states, even in highly confined regions (e.g., lipid rafts or membrane-protein clusters, intracellular vesicles, and synapses of neurons). For live-cell imaging (and unlike other methods), PHI allows the detection of very small metal NPs (D < 5 nm) in highly scattering environments with intensities that are compatible with cell integrity.

An image of live neurons with 5 nm gold-labeled glutamate receptors on its outer membrane is shown in Figure 5b. Because PHI requires a raster scan of the sample with integration time of a few milliseconds per point, fast imaging rates cannot be obtained readily, and moving objects are not resolved during the scan. Consequently, mobile receptors produce stripes

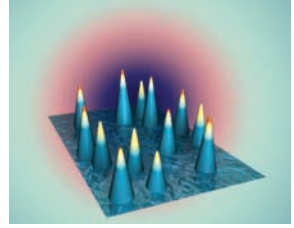

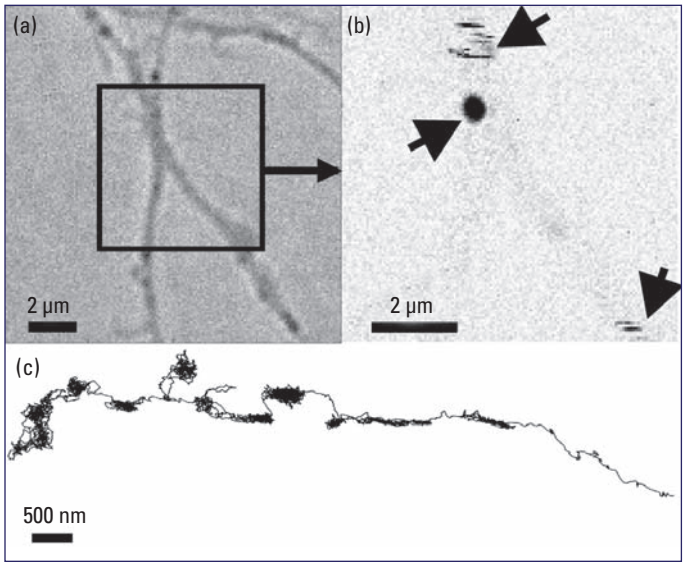

FIGURE 5. PHI of neurons.

(a) White light and (b) PHI images of live neurons labeled with AuNPs. The PHI image includes signals from one stationary and two moving membrane receptors labeled with AuNPs (arrows). (c) Trajectory of an individual receptor labeled with a 5 nm AuNP (>5 minutes, 9158 data points) acquired at video rate on a live neuron. (Go to http://pubs.acs.org/journals/ancham/multimedia/GluR2.mov to see another receptor diffusing on a neuron.)

of signal in the image, whereas immobile receptors are well resolved.

Lasne et al. recently designed a tracking scheme called single NP photothermal tracking (SNaPT) based on a triangulation from three measurement points to record the trajectories of single-membrane proteins labeled with AuNPs in live cells at video rates (*15*). The movement of single-membrane receptors could thus be recorded for several minutes (Figure 5c). Single-metal NP tracking combines the advantages of small marker size with practically unlimited observation times because of the high chemical stability of gold particles.

Improvements of the SNaPT method should allow the study of not only 2D movements of single molecules on cultured cells but also 3D movements in more complex systems, such as brain slices. For instance, the algorithm used in SNaPT can be easily generalized for tracking movements of NPs in 3D, and we foresee that the use of NIR excitation of small metal NPs or nanorods would be advantageous to go deeper into tissues.

Laurent Cognet is a senior research associate at Centre National de la Recherche Scientifique. His research interests include optical detection and spectroscopy of individual nano-objects and applications in neuroscience. Stéphane Berciaud is currently a postdoc at Columbia University. David Lasne is a graduate student at Université Bordeaux 1 working on single-molecule techniques in biology. Brahim Lounis is a professor at Université Bordeaux 1; his research interests include nano-optics, individual nano-object detection and spectroscopy, and applications in biology. Address correspondence to Lounis at b.lounis@cpmoh.u-bordeaux1.fr.

References

(1) Yguerabide, J.; Yguerabide, E. E. *Anal. Biochem.* **1998**, *262*, 137–156.
(2) Schultz, S.; et al. *Proc. Natl. Acad. Sci. U.S.A.* **2000**, *97*, 996–1001.
(3) Peyser, L. A.; et al. *Science* **2001**, *291*, 103–106.
(4) Liau, Y. H.; et al. *J. Phys. Chem. B* **2001**, *105*, 2135.
(5) Van Dijk, M. A.; Lippitz, M.; Orrit, M. *Acc. Chem. Res.* **2005**, *38*, 594–601.
(6) Van Dijk, M. A.; et al. *Phys. Chem. Chem. Phys.* **2006**, *8*, 3486–3495.
(7) Link, S.; El-Sayed, M. A. *Annu. Rev. Phys. Chem.* **2003**, *54*, 331–366.
(8) Wilcoxon, J. P.; et al. *J. Chem. Phys.* **1998**, *108*, 9137–9143.
(9) Tokeshi, M.; et al. *Anal. Chem.* **2001**, *73*, 2112.
(10) Boyer, D.; et al. *Science* **2002**, *297*, 1160–1163.
(11) Cognet, L.; et al. *Proc. Natl. Acad. Sci. U.S.A.* **2003**, *100*, 11,350–11,355.
(12) Berciaud, S.; et al. *Phys. Rev. Lett.* **2004**, *93*, 257402.
(13) Berciaud, S.; et al. *Phys. Rev. B* **2006**, *73*, 045424.
(14) Blab, G. A.; et al. *Biophys. J.* **2006**, *90*, L13–L15.
(15) Lasne, D.; et al. *Biophys. J.* **2006**, *91*, 4598–4604.
(16) Kreibig, U.; Vollmer, M. *Optical Properties of Metal Clusters*; Springer-Verlag: Berlin, 1995.
(17) Link, S.; El Sayed, M. A. *Int. Rev. Phys. Chem.* **2000**, *3*, 409–453.
(18) Persson, B. N. J. *Surf. Sci.* **1993**, *281*, 153–162.
(19) Bosbach, J.; et al. *Phys. Rev. Lett.* **2002**, *89*, 257404.
(20) Berciaud, S.; et al. *Nano Lett.* **2005**, *5*, 515–518.
(21) Klar, T.; et al. *Phys. Rev. Lett.* **1998**, *80*, 4249–4252.
(22) Prodan, E.; et al. *Science* **2003**, *302*, 419–422.
(23) Wuelfing, W. P.; et al. *J. Am. Chem. Soc.* **1998**, *120*, 12,696–12,697.
(24) Lounis, B.; et al. *Chem. Phys. Lett.* **2000**, *329*, 399.
(25) Leatherdale, C. A.; et al. *J. Phys. Chem. B* **2002**, *106*, 7619.
(26) Schlegel, G.; et al. *Phys. Rev. Lett.* **2002**, *88*, 137401.
(27) Efros, A. L., Lockwood, D. J., Tsybeskov, L., Eds. *Semiconductor Nanocrystals: From Basic Principles to Applications*; Kluwer Academic/Plenum Publishers: New York, 2003.
(28) Klimov, V. I.; et al. *Science* **2000**, *287*, 1011–1013.
(29) Berciaud, S.; Cognet, L.; Lounis, B. *Nano Lett.* **2005**, *5*, 2160–2163.
(30) Hartschuh, A.; et al. *Science* **2003**, *301*, 1354–1356.
(31) Cognet, L.; et al. *Science* **2007**, *316*, 1465–1468.
(32) O'Connell, M. J.; et al. *Science* **2002**, *297*, 593–596.
(33) Sfeir, M. Y.; et al. *Science* **2006**, *312*, 554–556.
(34) Islam, M. F.; et al. *Phys. Rev. Lett.* **2004**, *93*, 037404.
(35) Lauret, J. S.; et al. *Phys. Rev. Lett.* **2003**, *90*, 057404.
(36) Hertel, T.; Moos, G. *Phys. Rev. Lett.* **2000**, *84*, 5002–5005.
(37) Taton, T. A.; Mirkin, C. A.; Letsinger, R. L. *Science* **2000**, *289*, 1757–1760.
(38) Alexandre, I.; et al. *Anal. Biochem.* **2001**, *295*, 1–8.
(39) Fritzsche, W.; Taton, T. A. *Nanotechnology* **2003**, *14*, R63–R73.
(40) Park, S. J.; Taton, T. A.; Mirkin, C. A. *Science* **2002**, *295*, 1503–1506.
(41) Möller, R.; et al. *Nano Lett.* **2005**, *5*, 1475–1482.
(42) Zammatteo, N.; et al. *Biotechnol. Annu. Rev.* **2002**, *8*, 85–101.
(43) Sonnichsen, C.; et al. *Nat. Biotechnol.* **2005**, *23*, 741–745.
(44) Sheetz, M. P.; et al. *Nature* **1989**, *340*, 284–288.
(45) Ritchie, K.; et al. *Biophys. J.* **2005**, *88*, 2266–2277.
(46) Kusumi, A.; Sako, Y. *Curr. Opin. Cell Biol.* **1996**, *8*, 566–574.
(47) Borgdorff, A. J.; Choquet, D. *Nature* **2002**, *417*, 649–653.
(48) Cognet, L.; et al. *Sci. STKE* **2006**, *2006* (327), pe13.